LA-UR-99- 2689

96232

Approved for public release; distribution is unlimited

Title: **Innovative Composites Through Reinforcement Morphology Design–A Bone-Shaped-Short-Fiber Composites**

Author(s):

Yuntian T. Zhu	STC
James A. Valdez	MST-8
Irene J. Beyerlain	MST-8
Michael G. Stout	MST-8
Shujia Zhou	X-NH
Ning Shi	LANSCE
Terry C. Lowe	MST-DO

Submitted to: DOE Office of Scientific and Technical Information (OSTI)

RECEIVED
SEP 07 1999
OSTI

Los Alamos
NATIONAL LABORATORY

Los Alamos National Laboratory, an affirmative action/equal opportunity employer, is operated by the University of California for the U.S. Department of Energy under contract W-7405-ENG-36. By acceptance of this article, the publisher recognizes that the U.S. Government retains a nonexclusive, royalty-free license to publish or reproduce the published form of this contribution, or to allow others to do so, for U.S. Government purposes. Los Alamos National Laboratory requests that the publisher identify this article as work performed under the auspices of the U.S. Department of Energy. Los Alamos National Laboratory strongly supports academic freedom and a researcher's right to publish; as an institution, however, the Laboratory does not endorse the viewpoint of a publication or guarantee its technical correctness.

Form 836 (10/96)
ST 2629

DISCLAIMER

This report was prepared as an account of work sponsored by an agency of the United States Government. Neither the United States Government nor any agency thereof, nor any of their employees, make any warranty, express or implied, or assumes any legal liability or responsibility for the accuracy, completeness, or usefulness of any information, apparatus, product, or process disclosed, or represents that its use would not infringe privately owned rights. Reference herein to any specific commercial product, process, or service by trade name, trademark, manufacturer, or otherwise does not necessarily constitute or imply its endorsement, recommendation, or favoring by the United States Government or any agency thereof. The views and opinions of authors expressed herein do not necessarily state or reflect those of the United States Government or any agency thereof.

DISCLAIMER

Portions of this document may be illegible in electronic image products. Images are produced from the best available original document.

Innovative Composites Through Reinforcement Morphology Design–A Bone-Shaped-Short-Fiber Composite

Yuntian T. Zhu*, James A. Valdez, Irene J. Beyerlain, Michael G. Stout, Shujia Zhou, Ning Shi, and Terry C. Lowe

Abstract

This is the final report of a three-year, Laboratory Directed Research and Development (LDRD) project at Los Alamos National Laboratory (LANL). The objective of this project is to improve the strength and toughness of conventional short-fiber composites by using innovative bone-shaped-short (BSS) fibers as reinforcement. We fabricated a model polyethylene BSS fiber-reinforced polyester-matrix composite to prove that fiber morphology, instead of interfacial strength, solves this problem. Experimental tensile and fracture toughness test results show that BSS fibers can bridge matrix cracks more effectively, and consume many times more energy when pulled out, than conventional-straight-short (CSS) fibers. This leads to both higher strength and fracture toughness for the BSS-fiber composites. A computational model was developed to simulate crack propagation in both BSS- and CSS-fiber composites, accounting for stress concentrations, interface debonding, and fiber pullout. Model predictions were validated by experimental results and will be useful in optimizing BSS-fiber morphology and other material system parameters.

Background and Research Objectives

Engineered composite materials are well known for their superior properties. For instance, fiber-reinforced composites have superior mechanical properties over their unreinforced matrix. For civilian applications, cost is often a deciding factor in materials selection. Compared with continuous fiber composites, short-fiber composites are cost effective because they can be adapted to conventional manufacturing techniques [1-4]. However, the application of short-fiber composites has so far been limited primarily to light-load-bearing components, because of their low strength and toughness.

The relatively low strength and toughness of short-fiber composites are intrinsic problems caused by two main factors. First, numerous discontinuities provided by fiber ends can produce stress concentrations on nearby fibers and promote matrix microcracking at these ends. These microcracks, which occur even prior to fiber failure, most likely

*Principal Investigator, e-mail: yzhu@lanl.gov

coalesce to form a large main crack. Second, the fiber/matrix interface is often a limiting factor for improving mechanical properties of short-fiber composites [5-8]. With respect to interface selection, there exists a trade off between the strength and toughness of short-fiber composites: high strength is often obtained at the sacrifice of toughness. For a short-fiber composite, a strong interface is desirable to transfer load from matrix to fibers, since relatively stronger interfaces can increase the effective fiber length over which the fiber carries load [9-11]. However, strong interfaces and nearby fiber ends can produce stress concentrations, which induce fiber failure rather than fiber bridging and pull-out, particularly in response to an approaching crack [12,13]. Even for composites with highly ductile matrices, such as metal and polymer matrices, strong interfaces will promote successive breakage of adjacent fibers [13], and interfacial debonding and matrix crack bridging are not dominating failure mechanisms [14]. Weak interfaces, on the other hand, can reduce stress concentrations in a short fiber by debonding. However, they also significantly decrease the effective length of the fiber that carries load, rendering the fiber ineffective in strengthening the matrix. Extremely weak interfaces may result in *complete* fiber interfacial debonding and pullout, producing a significant loss in composite strength with no or minimal improvement in composite toughness.

The objective of this project is to prove an innovative concept that fiber morphology, instead of interfacial strength, solves the low strength and toughness problem of short -fiber composites. To fully understand and utilize the potential of the bone-shaped reinforcement geometry, a combined experimental/modeling effort was undertaken.

Importance to LANL's Science and Technology Base and National R&D Needs

The fabrication, testing, and modeling of the BSS-fiber/polyester composite conducted in this project open a new field in the research and development of short-fiber composites. The innovative bone-shaped short fibers provide a possibility to make short-fiber composites with balanced high strength and toughness. The fundamental insights obtained from this experimental/modeling study can be applied to other bone-shaped short-fiber composite systems. Since a news release on this project, we have found significant interests in this technology from the defense sector, industry and academia.

This project directly supports two Laboratory core competencies: nuclear and advanced materials; and theory, modeling and high performance computing. The BSS-fiber composites have high strength and toughness at low costs. They can be used for applications that need lightweight and sturdy structural parts, which include nuclear weapon applications. The micromechanical modeling in this project supports microstructural modeling capabilities that are currently under development within the

materials modeling portion of the Accelerated Strategy Computing Initiative (ASCI) program. This same modeling capability should be extensible to work for several offices within DOE/EE in which we are developing advanced lightweight materials to improve energy efficiency in transportation systems.

Scientific Approach and Accomplishments

Scientific Approach

A. Experimental Procedure

BSS fibers from both pure Ni and polyethylene filaments were processed in our laboratory (see Refs. 15 and 16). CSS fibers were prepared using a pair of scissors. Tensile and double cantilever beam (DCB) test specimens of short-fiber reinforced polyester matrix were fabricated with well-aligned short fibers [15-17]. The tensile specimens were for measuring composite strength, while the DCB specimens were for measuring fracture toughness (the ability of the composites to resist crack propagation). In addition, single-fiber pullout tests were also performed to compare the pull-out resistance and consumed energies of the BSS and CSS fibers and to estimate fiber-matrix interfacial strength for subsequent modeling. Readers are referred to Ref. 15-17 for more details on the fabrication of these specimens.

Tensile testing was performed using an Instron testing machine. An extensometer was used to measure strain. A constant strain rate of 0.0001 s^{-1} was employed for all samples. Fracture surface was investigated using a JEOL 6300FXV Scanning Electron Microscope (SEM). An optical microscope was used to investigate fiber alignment.

B. Modeling of Crack Resistance

A physical model was developed to represent crack propagation in short fiber composites from an initial notch. Using the computational implementation of the model, we can investigate how short-fiber length, morphology, elastic properties, strength distribution, volume fraction, and the interface properties control composite strength and toughness. The model assumes that the fibers sustain all axial stress and the matrix deforms only in shear.

An inhomogeneous stress state is generated under loading due to interactions between the randomly spaced fiber ends. Tensile and shear stress concentrations can promote microcrack formation at the fiber ends and subsequent sliding at the fiber/matrix interface. Short fibers remain intact during the fracture process and the macroscopic response is thus dominated by fiber bridging and pullout. All these features seen experimentally are incorporated into the computational model. To accurately represent the experimental results, we need the limiting shear stress at which the fiber/matrix interface

separates, the interfacial shear stress for when the fiber is sliding relative to the matrix, and the critical displacement at which fiber ends separate from the matrix. Readers are referred to Ref. 17 for more details.

Accomplishments

Our experimental results demonstrate that the bone-shaped-short (BSS) fiber composites have simultaneously both high strength and high toughness. This is what has been pursued but not been obtained for the last few decades by scientists and engineers working on short-fiber composites. Computational modeling closely agrees with experimental data that shows high effectiveness of BSS fibers in bridging cracks. Good crack bridging results in high fracture toughness and prevents catastrophic material failure. We present more details in the following sections.

A. Experimental Results

A-1 Tensile Properties

In Figure 1 are pictures of (a)-(c) BSS-fiber and (d) CSS-fiber reinforced composite specimens during tensile testing. Figure 1a shows that at 5% strain, the surface of the BSS-fiber reinforced composite specimen became rough. The rough surface was caused by the non-uniform stress state of the polyester matrix as a result of the spatial variation in the location of the fibers. In the failure process, some of the BSS fibers contributed to forming the crack and some contributed to bridging the crack and eventually were pulled out. Matrix crack formation was found to be more likely in regions where several ends were roughly aligned along a plane perpendicular to the straining direction. The arrow in Fig. 1a indicates such a weak cross-section of high local stress concentration, appearing as a linear surface groove across the specimen surface.

Upon further straining, a matrix crack was initiated at this site (Figure 1b), but was effectively bridged by BSS fibers to prevent catastrophic failure of the specimen. The surface area directly above and below the crack is smooth due to stress relaxation in these areas, while the surface away from the crack is rather rough. As the specimen was further strained, it became bent as the main matrix crack propagated in a stable manner from left to right with BSS fibers pulling out in its wake, and a second matrix crack developed (see arrow in Figure 1c). In contrast, CSS fibers could not as effectively bridge the matrix crack, resulting in immediate pull out and sample failure once a matrix crack formed (Figure 1d). In both cases, the fibers did not fracture and composite strength was dominated by matrix crack initiation at fiber ends and fiber bridging and pull-out.

What we have discussed above is the macroscopic observation of the tensile failure process of BSS- and CSS-fiber composites. More insightful information can be obtained from microscopic fractographs of these composites (Figures 2 and 3). For the BSS-fiber composites, the crack usually initiated at fiber ends (Figure 2a), or at surface flaws on the specimen (see arrow in Figure 2b). The main crack propagated by coalescing with small cracks formed at nearby BSS-fiber ends. The smaller cracks were often not on the same plane as the larger crack, resulting in a very rough fracture surface. Because of the processing technique used in this study, the ends of BSS fibers were usually disk-shaped, with their broad face perpendicular to the longitudinal axis of the fiber. When a composite specimen was loaded in tension, each fiber end acted much like a crack oriented perpendicular to the loading direction. Though the bulk polyester matrix can sustain relatively large deformations, the complex, triaxial stress state of the matrix material in the composite makes the matrix crack sensitive. When a matrix crack is initiated at a fiber end, the polyester matrix behaves in a brittle manner, as evidenced by the river-marks in fractographs of both BSS- and CSS- fiber composites (Figures 2 and 3, respectively). These river-marks are similar to that on the fractured surface of a typical brittle ceramic material. As a crack propagates, some BSS fibers bridging the crack might be pulled out, which is a difficult process because of the enlarged ends. The pullout process consumed large amounts of energy, since it resulted in extensive damage to the matrix (Figure 2c).

Figure 3 shows the fractographs of several CSS-fiber composite samples. Figure 3a shows a fracture surface that formed from a crack initiated at a fiber end (see the arrow mark). The small crack propagated slowly at the beginning, leaving a smooth mirror-like area. Once the crack grew to a critical size, it propagated quickly across the whole specimen, leaving a relatively flat fracture surface with river marks. Figure 3b shows a case of initial crack formation from clustered fiber ends (see arrows in the figure). No smooth mirror zone associated with slow crack propagation can be seen, apparently because the crack grew to an unstable size by coalescence of several small cracks. Once the crack reached a critical size, it propagated through the entire cross section of the sample, pulling out fibers in its wake. It can be seen from the river marks that the sample failed from a single crack (Figure 3b). This is consistent with the observation in Figure 1 that the crack propagated quickly after its formation. In contrast to BSS fibers, the pullout of CSS fibers did not result in much matrix damage (Figure 3c), which means less energy was consumed during the pullout process.

The different failure processes of the BSS- and CSS-fiber composites have a significant effect on their mechanical response under tensile loading, as revealed in the strain-stress curves shown in Figure 4. The maximum strengths measured for each

Table I. The maximum strengths of the BSS- and CSS-fiber composites (fiber length ℓ= 3.0 and 4.5 mm, respectively). The matrix stress at the circle on the stress-strain curve is 11.5 MPa.

	Composite strength σ_c (MPa)			
Sample #	ℓ = 3.0 mm		ℓ = 4.5 mm	
	BSS	CSS	BSS	CSS
1	14.6	13.7	16.7	13.8
2	14.8	13.5	16.0	13.3
3	14.8	12.3	16.5	13.0
Average	14.7	13.2	16.4	13.4

sample are indicated by the circles on these stress-strain curves and are also listed in Table I. First, despite the relatively small volume fraction V_f and short fiber length ℓ, these BSS fibers were extremely effective in strengthening the bulk matrix material. Second, the average strengths of the BSS-fiber composites are greater than CSS-fiber composites by 11.1% and 22.4% for samples with ℓ= 3.0 and 4.5 mm, respectively. The strengths of both BSS- and CSS-fiber composites should approach the strength of continuous fiber composites as ℓ increases further and likewise approach the strength of particulate-reinforced composites as ℓ decreases. Therefore, although the difference in strength between the BSS- and CSS-fiber composites may continue to increase (as shown in Table I), it will eventually decrease with increasing ℓ. In other words, we expect there exists an optimum ℓ at which BSS-fiber composites will have the largest improvement in strength over CSS-fiber composites for a given material system.

One salient feature of the strain-stress curves of BSS-fiber composites is the gradual stress decrease with increasing strain at composite failure. This is in sharp contrast to the strain-stress curves of the CSS-fiber composite, in which the stress suddenly dropped to zero at composite failure. This is consistent with the observations seen in Figure 1 that cracks propagated in a stable manner in the BSS-fiber composites, but cause catastrophic failure in the CSS-fiber composites. This reduced crack sensitivity of the BSS-fiber composites is provided by the effective crack-bridging capability of the enlarged BSS fiber ends. One of the strain-stress curves of BSS-fiber composites in Figure 4b shows three abrupt stress drops (see arrows). The first drop occurred at 3.5% strain, which was

probably caused by the initiation of a crack. Afterwards, the composite sample was able to sustain higher stresses at larger applied strains due to the effective crack-bridging of BSS fibers. The second stress drop at 7% strain was caused by either the formation of a new crack or sudden propagation of an existing crack. The stress plateau following the second stress drop suggests that the crack was also effectively arrested by BSS fibers. Finally at 11% strain, the BSS fibers could no longer prevent the propagation of the large crack, which led to a gradual stress decrease with increasing strain.

A-2 Effective Stress Analysis

The benefit of BSS fibers is also revealed when considering a simple "effective fiber stress" analysis using data from Table 1. In this analysis, these composite samples can be approximately considered as reinforced by unidirectional short fibers. The average fiber stress at maximum composite strength, σ_{ef}, can be approximated from a simple rule-of-mixtures [19] as

$$\sigma_{ef} = \left[\sigma_c - \left(1 - V_f\right)\sigma_m\right] / V_f \quad (1)$$

where σ_c is the maximum strength of the composites (See Table 1), V_f is the fiber volume fraction, and σ_m is the stress in matrix at which the maximum composite strength is measured (see Figure 4 and Table 1).

In both the BSS- and CSS-fiber composites, V_f and ℓ were the same; however, their σ_{ef} must be interpreted differently. For a BSS fiber, σ_{efb} is the average stress along the fiber, assuming ℓ equals the volume of the fiber divided by its cross-section. This assumption slightly overestimates the actual ℓ of the BSS fiber because of the volume associated with its enlarged ends. For the same ℓ, a BSS fiber has a larger volume than a CSS fiber because of its enlarged mushroom-shaped ends. Also, the larger volume of the BSS fibers leads to a smaller number of fibers per unit volume in BSS-fiber composites than in CSS-fiber composites for the same V_f, as is the case in this study. So given α, the volume ratio of a BSS fiber to a CSS fiber, the relationship between the actual effective fiber stress, σ^a_{efb}, and σ_{efb} can be expressed as

$$\sigma^a_{efb} = \alpha\sigma_{efb} \quad (2)$$

For the polyethylene fibers used in this study, $\alpha = 1.27$ for $\ell = 3$ mm and $\alpha = 1.18$ for $\ell =$ 4.5 mm and thus, σ^a_{efb} is larger than σ_{efb} calculated by Eq. 1.

Using the average maximum strength data from Table I, the effective fiber stress, σ_{efb}, and actual effective fiber stress, σ^a_{efb}, for the BSS-fiber composites and the effective fiber stress, σ_{efc}, for the CSS-fiber composites, are calculated using Eqs. 1 and 2, and listed in

Table II. The effective fiber stress σ_{efb}, and actual effective fiber stress σ^a_{efb} for BSS-fiber composites and the effective fiber stress σ_{efc}, for CSS-fiber composites as calculated using Eqs. 1 and 2.

Fiber length ℓ	ℓ=3.0 mm	ℓ=4.5 mm
σ_{efb} (MPa)	71.7	116.5
σ^a_{efb} (MPa)	91.1	137.4
σ_{efc} (MPa)	41.7	53.3
$\sigma_{efb}/\sigma_{efc}$	1.72	2.19
$\sigma^a_{efb}/\sigma_{efc}$	2.18	2.58

Table II. It can be seen that the ratio of effective fiber stress in BSS fibers to that in CSS fibers, $\sigma_{efb}/\sigma_{efc}$, is 1.72 when $\ell = 3.0$ mm, and increases to 2.19 when $\ell = 4.5$ mm. The ratio $\sigma^a_{efb}/\sigma_{efc}$ is 2.18 when $\ell = 3.0$ mm, and increases to 2.58 when $\ell = 4.5$ mm. In other words, a BSS fiber with the geometry used in this study is 118% more effective than a CSS fiber in improving composite strength when $\ell = 3.0$ mm, and 158% more effective when $\ell = 4.5$ mm.

A-3 Crack Propagation Resistance

In order to investigate the fracture toughness of the CSS-fiber composites and BSS-fiber composites and crack-bridging effectiveness of the BSS fibers, DCB samples were fabricated and tested. The total normalized energy consumed for a crack to propagate from the initial crack length a_0 to crack length a can be calculated as

$$E(a) = \int_0^{v(a)} \overline{P}(v)dv \tag{3}$$

where $\overline{P}$ (v) is the normalized load as a function of crack opening displacement, $v(a)$, along the loading line. Each measured crack length a corresponds to a displacement $v(a)$. Shown in Figure 5a are the total normalized energies $E(a)$ calculated by Eq. 3 as a function of crack length for DCB tests of both BSS- and CSS-fiber composites. As shown, $E(a)$ is higher for BSS-fiber composites than for CSS-fiber composites.

The supplied energy for a crack to propagate by a unit length can be calculated by

$$\varepsilon(a) = \frac{dE(a)}{da} \tag{4}$$

Using Eq. 4, $\varepsilon(a)$ was calculated and is shown in Figure 5b. For both types of DCB specimens, $\varepsilon(a)$ is an increasing function of a. Also note that $\varepsilon(a)$ includes energies consumed both by crack propagation and by further deformation in the two beams of the DCB specimen, which makes it larger than the crack resistance, R, or the energy consumption in the formation of a unit length of crack. As shown, the BSS-fiber DCB specimens require significantly more energy for crack propagation than the CSS-fiber DCB specimens. Since the fibers did not fracture this enhanced crack resistance, or (indirectly) higher fracture toughness of the BSS-fiber composites, is due solely to their enhanced ability to bridge matrix cracks and to resist pull-out.

A-4 Single Fiber Pullout

Single fiber pullout tests were performed to compare the crack bridging capability of a BSS fiber with a CSS fiber. Figure 6 shows the load (F) versus pull-out displacement (u) curves of both BSS and CSS fibers for two different embedded lengths, 3.5 mm and 6.4 mm. The free length, $L_0 = 20$ mm, was the same in both cases. For these embedded lengths, the fiber was fully pulled-out and did not break.

In all cases, the peak load F_{max} and energy consumption for pulling out a BSS fiber are much higher than those for pulling out a CSS fiber. For the pullout tests with embedded fiber length $L_e = 3.5$ mm (Fig. 6a), F_{max} for pulling out a BSS fiber is 9 times that for pulling out a CSS fiber. When L_e was increased from 3.5 mm to 6.4 mm (Fig. 6b), F_{max} for pulling out BSS fibers increased by only 10%. In contrast, F_{max} for pulling out CSS fibers increased by more than 150%. The total energy consumed during fiber pullout, or the area under these load-displacement curves, also increases with L_e, following a trend similar to that observed for F_{max}. For $L_e = 3.5$ mm, the BSS fiber consumed 17 times more energy than the CSS fiber. When L_e was increased from 3.5 mm to 6.4 mm,

energy consumption increased by 70% for BSS fibers, as compared with 400% for CSS fibers.

The substantial difference in the effect of L_e between the CSS and BSS fibers on F_{max} and energy consumption is due to the difference in their pull-out failure mechanisms. The CSS fiber response depends primarily on the fiber-matrix interface integrity, which results in much more dependence of F_{max} on L_e. Increasing L_e will increase F_{max} because of the increased fiber-matrix interface area associated with debonding. In contrast, the BSS fiber response depends on its enlarged end, which directly leads to a higher F_{max} prior to the extraction process. The contribution from increasing L_e or interface area is relatively small as compared to that associated with mechanical locking of the enlarged BSS fiber end with the matrix. However, these results suggest that these relative differences between the BSS and CSS fibers will decrease with increasing L_e.

B. Modeling Results

Figure 7 compares the opening displacement (CTOD) at the mouth of the initial notch versus the amount of crack extension, $\Delta a_c/(h+d) = n_c$, for the BSS- and CSS-fiber composites, where $N = 50$, $n_s = 75$ and $\ell = 7.0$ mm. For each type of composite, five curves are shown, representing five composites with different random fiber spatial distributions. (Plots of normalized applied load $\overline{P}$ versus Δa_c or Δa_b show similar trends.) Prior to or at initial crack extension, many failure mechanisms, such as fiber end detachment and fiber sliding can occur ahead of the initial notch. Variation among the BSS- or the CSS-fiber composite curves is due solely to the statistical variation in locations of fiber ends with respect to the crack. Also the sharp rise in CTOD as the crack propagates to a length n_c ~60-70 is due to boundary constraints provided by the intact fibers, i.e. fibers $n > 75$. This boundary effect also occurs in the DCB specimens and is neglected when comparing the BSS- and CSS-fiber composites.

Figure 7 reveals the effectiveness of the BSS fibers. Prior to the sharp rise at the end, the CTOD of the CSS-fiber composites does not increase appreciably above the short fiber length, $\ell = 7.0$ mm. However, a much larger (approximately 2.5 ~ 3.0 times larger) CTOD is required to drive crack extension and complete pull-out in the BSS-fiber composites than in the CSS-fiber composites. Also, although it appears that the variation in the response of the BSS-fiber composite is much larger, the coefficient of variation (or standard deviation to mean ratio) in the CTOD of the BSS-fiber composite at n_c ~60 is slightly smaller (0.2902 versus 0.3032). This suggests that the CSS- and BSS-fiber

composites have nearly the same sensitivity in crack propagation to variation in fiber spatial distribution.

To reveal the damage occurring ahead of the growing Δa_c or Δa_b, graphic 'snapshots' of an increment in the simulation for a CSS and a BSS-fiber specimen at approximately the same far-field normalized load (~17) are shown in Figure 8. As indicated, fiber ends are in one of three states: (i) intact, (ii) debonded, and (iii) debonded and sliding. On the crack plane, $z = 0$, the fiber status is represented by two states: (iv) bridging (at least one sliding and debonded end) and (v) pulled-out short fibers. At this value of $\overline{P}$, the matrix crack in the CSS-fiber composites has already propagated to the end and contains a majority of pulled-out fibers. The BSS-fiber composite, on the other hand, contains a relatively smaller bridging zone at this applied load, which in general contains both bridging and pulled-out fibers. Note that there are also a number of fibers ahead of the crack that have already been pulled out, and this damage tends to occur near fibers with ends clustered near the crack plane. The stress concentrations from the approaching crack most often promote premature microcracking in these areas, even if they are far from the crack-tip. When encountered by the approaching crack, these areas will lead to immediate crack extension or discrete steps in $\overline{P}$ vs a_c or a_b curves. Significantly, these results are consistent with trends observed in DCB specimen tests.

C. Summary

BSS-fiber composites have proven to have both higher strength and toughness than CSS-fiber composites. By using enlarged ends to transfer load, BSS fibers allow a weak interface to be used without compromising the effectiveness of load transfer from matrix to fiber. This avoids the dilemma in CSS-fiber composites, in which a weak interface leads to low strength because of ineffective load transfer but a strong interface results in low toughness because of stress concentration.

Interfacial debonding along a BSS fiber does not affect its load carrying capability, making BSS fibers very effective in bridging a crack. This leads to higher fracture toughness for BSS-fiber composites. Another factor that contributed to the effectiveness of BSS fibers is the fact that the fibers in these composites did not fracture. This is because the BSS fiber ends are not large enough to prevent the fiber from being pulled out before it is broken. The critical size of BSS-fiber ends that govern the transition from a fiber being pulled out to being broken is influenced by the mechanical properties and geometry of the fiber and the properties of the matrix and interfaces.

The crack sensitivity of the polyester matrix has played a major role in crack formation in the BSS-fiber composites. The mushroom-cap geometry of BSS fibers, coupled with the high crack sensitivity of the matrix, led to the failure of BSS-fiber composites primarily by crack initiation and coalescence. This mode of failure can only utilize a small portion of the reinforcing and crack bridging potential of BSS fibers. Although the matrix in bulk can sustain large plastic strains, it behaves more like a brittle material once a crack has formed. Therefore, we propose that ellipsoidal fiber ends and a less crack-sensitive matrix will suppress crack formation and further increase the strength and toughness of BSS-fiber composites. Overall, the results show that it will be worthwhile to develop commercial BSS-fiber composites with weak interfaces, test their mechanical properties, and perform computational modeling for optimum fiber shape and length.

Publications

1. Taylor, S.T., Zhu, Y.T., Blumenthal, W.R., Stout, M.G., Butt, D.P., and Lowe, T.C., "Characterization of Nicalon Fibers with Varying Diameters. Part I: Strength and Fracture Studies," *Journal of Materials Science,* **33**, 1465-73 (1998).

2. Zhu, Y.T., Taylor, S.T., Stout, M.G., Butt, D.P., Blumenthal, W.R., and Lowe, T.C., "Characterization of Nicalon Fibers with Varying Diameters. Part II: Modified Weibull Distribution," *Journal of Materials Science*, **33**, 1475-80 (1998).

3. Taylor, S.T., Zhu, Y.T., Butt, D. P., Stout, M. G., Blumenthal, W.R., and Lowe, T.C., "Some New Perspectives on the Strength and Fracture of Nicalon Fibers," *Proceedings of Third International Conference on Composite Engineering*, New Orleans, July 21-27, 1996, pp. 837-838.

4. Zhu, Y.T., Blumenthal, W.R., Stout, M.G., and Lowe, T.C., "Modeling of Statistical Tensile Strength of Short-Fiber Composites," *Modeling of Composites: Processing and Properties*, edited by S. P. Chen and M. P. Anderson, TMS, pp. 11-21 (1996).

5. Zhu, Y.T., Blumenthal, W.R., and Lowe, T.C., "Determination of *Non-Symmetric* 3-D Fiber Orientation and Average Fiber Length in Short-Fiber Composites," *J. Composite Materials*, **31**, 1287-1301 (1997).

6. Zhu, Y.T., Blumenthal, W.R., Stout, M.G., and Lowe, T.C., "Modeling of Young's Modulus of Composites Reinforced with 3-D Oriented Short Fibers," Physical Properties of Composites, edited by R. Pitchumani and P. K. Liaw, TMS, pp. 37-40 (1996).

7. Zhu, Y.T., Blumenthal, W.R., Stout, M.G., and Lowe, T.C., "The Tensile Strength of Short Fiber-Reinforced Composites," *J. Materials Science,* **32**, 2037-43 (1997).

8. Taylor, S.T., Zhu, Y.T., Butt, D. P., Stout, M. G., Blumenthal, W.R., and Lowe,

T.C., "New Perspectives on the Fracture of Nicalon Fibers," *Special Technical Publication (STP) 1332,* ASTM, **29**, **XXX-XXX (199X)**.

9. Zhu, Y.T., Taylor, S.T., Stout, M.G., Butt, D.P., and Lowe, T.C., "Kinetics of Thermal, Passive Oxidation of Nicalon Fibers," *J. American Ceramic Society* , **81**, 655-60 (1998).

10. Zhu, Y.T., Butt, D.P., Taylor, S.T., and Lowe, T.C., "Evaluation of a Modified Weibull Distribution in Characterizing the Strength of Ceramic Fibers and Whiskers with Varying Diameters," *J. Testing and Evaluation* , **26**, 144-150 (1998).

11. Zhu, Y.T., Taylor, S.T., Stout, M.G., Butt, D.P., Blumenthal, W.R., and Lowe, T.C., "On the Statistical Strength of Nicalon Fibers and its Characterization," *Ceramic Engineering and Science*, **18**, 119-126 (1997).

12. Zhu, Y.T., Valdez, J.A., Shi, N., Lovato, M.L., Stout, M.G., Zhou, S., Blumenthal, W.R., and Lowe, T.C., "Influence of Reinforcement Morphology on the Mechanical Properties of Short-Fiber Composites," Processings of Metals and Advanced Materials: Modeling, Design and Properties. Edited by B. Q. Li, TMS, 1998, pp. 251-259.

13. Zhu, Y.T., Valdez, J.A., Shi, N., Lovato, M.L., Stout, M.G., Zhou, S., Blumenthal, W.R., and Lowe, T.C., "A Composite Reinforced with Bone-Shaped Short Fibers," *Scripta Materialia* (in press).

14. Zhu, Y.T., Valdez, J.A., Beyerlein, I.J., Zhou, S., Liu, C., Stout, M.G., Butt, D.P., and Lowe, T.C., "Mechanical Properties of Bone-Shaped-Short-Fiber Reinforced Composites," Acta Materialia (in press).

References

[1] Chen, P.E. *Polymer Eng. and Sci.,* **11,** 51 (1971).

[2] Liaw, P.K., Greggi, J.G. and W.A. Logsdon, *J. Mater. Sci.,* **22**, 1613 (1987).

[3] Gaggar, S.K. and Broutman, L.J., *Polymer Eng. and Sci.*, **16**, 537 (1976).

[4] Klimowicz, T.F., *J. of Metals*, **November**, 49 (1994).

[5] Crasto, A., Own, S.H. and Subramanian, R.V., Composite Interfaces, Ishida, H. and Koenig, J. L., eds., p. 133, Elsevier Science Publishers, New York (1986).

[6] Fishkis, M., Yeh, J.R., and Wefers, K., *J. Mater. Sci.*, 29, 110 (1994).

[7] Feest, E.A., *Composites*, **25,** 75 (1994).

[8] Kunz, S.M., Chia, K., McMurtry, C.H., and Boecker, W.D.G., Composite Applications, Drozda, T.J., ed., p. 38, Society of Manufacture Engineers, Dearborn, Michigan (1989).

[9] Friend, C.M., *Scripta Metall.*, **23**, 33 (1989).

[10] Xia, K. and Langdon, T.G., *J. Mater. Sci.*, **29**, 5219 (1994).

[11] Zhu, Y.T., Zong, G., Manthiram, A., and Eliezer, E., *J. Mater. Sci.*, **29**, 6281 (1994).

[12] Yasuda, E., Akatsu, T., Tanabe, Y., and Matsuo, Y., Composite Materials, A. T. Benedetto, Nicolais, L., and Watanabe, R., eds., p. 167, Elsevier Science Publishers, New York (1992).

[13] Norita, T., Matsui, J., and Matsuda, H.S., Composite Interfaces, Ishida, H. and Koenig, J. L., eds., p. 123, Elsevier Science Publishers, New York (1986).

[14] Kelly, A. and Tyson, W.R., *J. Mech. Phys. Solids*, **13**, 239 (1965).

[15] Zhu, Y.T., Valdez, J.A., Shi, N., Lovato, M.L., Stout, M.G., Zhou, S., Blumenthal, W.R., and Lowe, T.C., "Influence of Reinforcement Morphology on the Mechanical Properties of Short-Fiber Composites," Processings of Metals and Advanced Materials: Modeling, Design and Properties. Edited by Li, B.Q., TMS, 1998, pp. 251-259.

[16] Zhu, Y.T., Valdez, J.A., Shi, N., Lovato, M.L., Stout, M.G., Zhou, S., Blumenthal, W.R., and Lowe, T.C., "A Composite Reinforced with Bone-Shaped Short Fibers," *Scripta Materialia* (in press).

[17] Zhu, Y.T., Valdez, J.A., Beyerlein, I.J., Zhou, S., Liu, C., Stout, M.G., Butt, D.P., and Lowe, T.C., "Mechanical Properties of Bone-Shaped-Short-Fiber Reinforced Composites," Acta Materialia (in press).

[18] Zhu, Y.T., Blumenthal, W.R., and Lowe, T.C., *J. Composite Materials*, **31**, 1287 (1997).

[19] Zhu, Y.T., Blumenthal, W.R., and Lowe, T.C., *J. Mater. Sci.,* **32**, 2037 (1997).

[20] Fukuda, H. and Chou, T.W., *J. Mater. Sci.*, **16**, 1088 (1981).

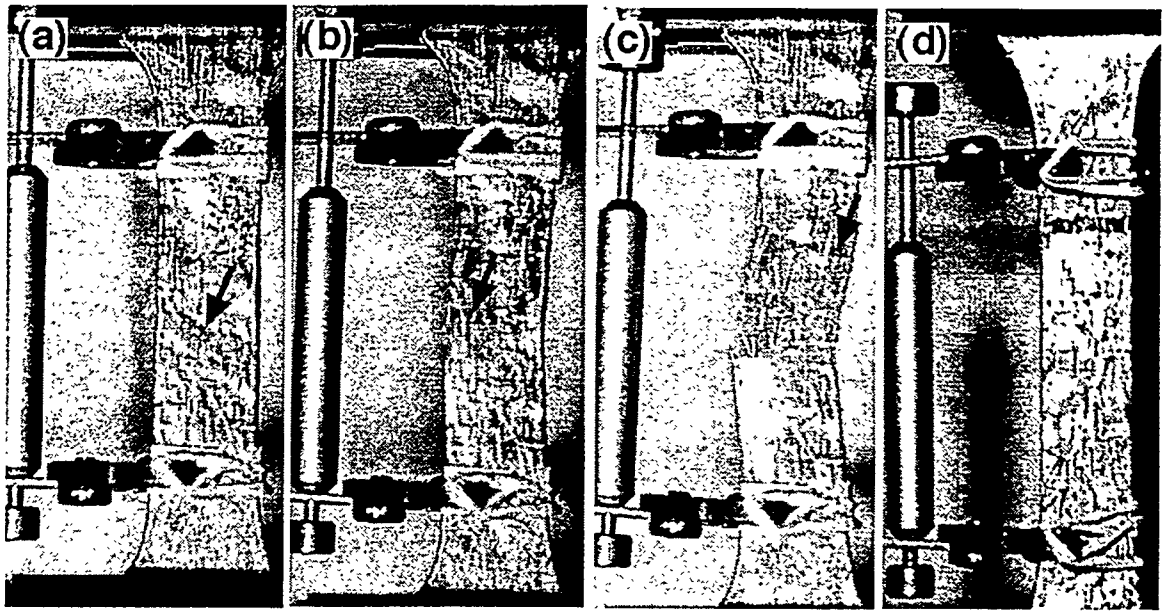

Figure 1: *In situ* pictures of (a) - (c) BSS-fiber reinforced and (d) CSS-fiber reinforced tensile specimens during tensile testing. The engineering strain states are (a) 5%, (b) 13%, (c) 20% and (d) 25%.

Figure 2: SEM micrographs of fracture surfaces of BSS-fiber composites.

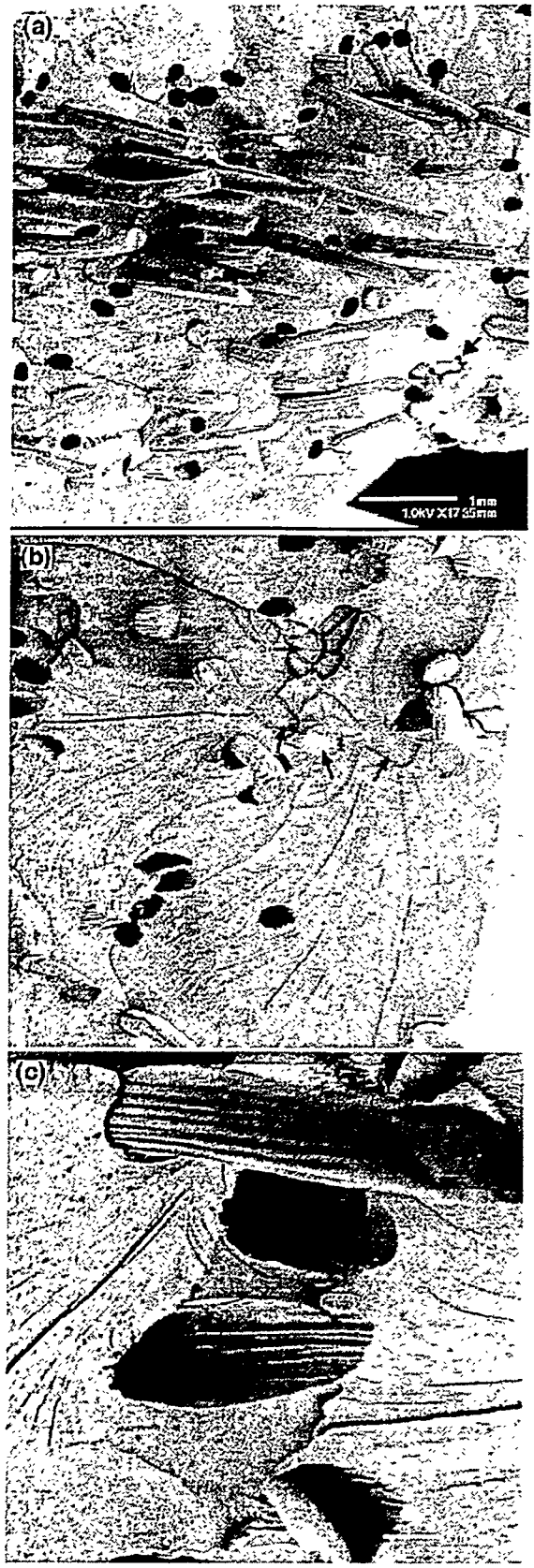

Figure 3: SEM micrographs of fracture surfaces of CSS-fiber composites.

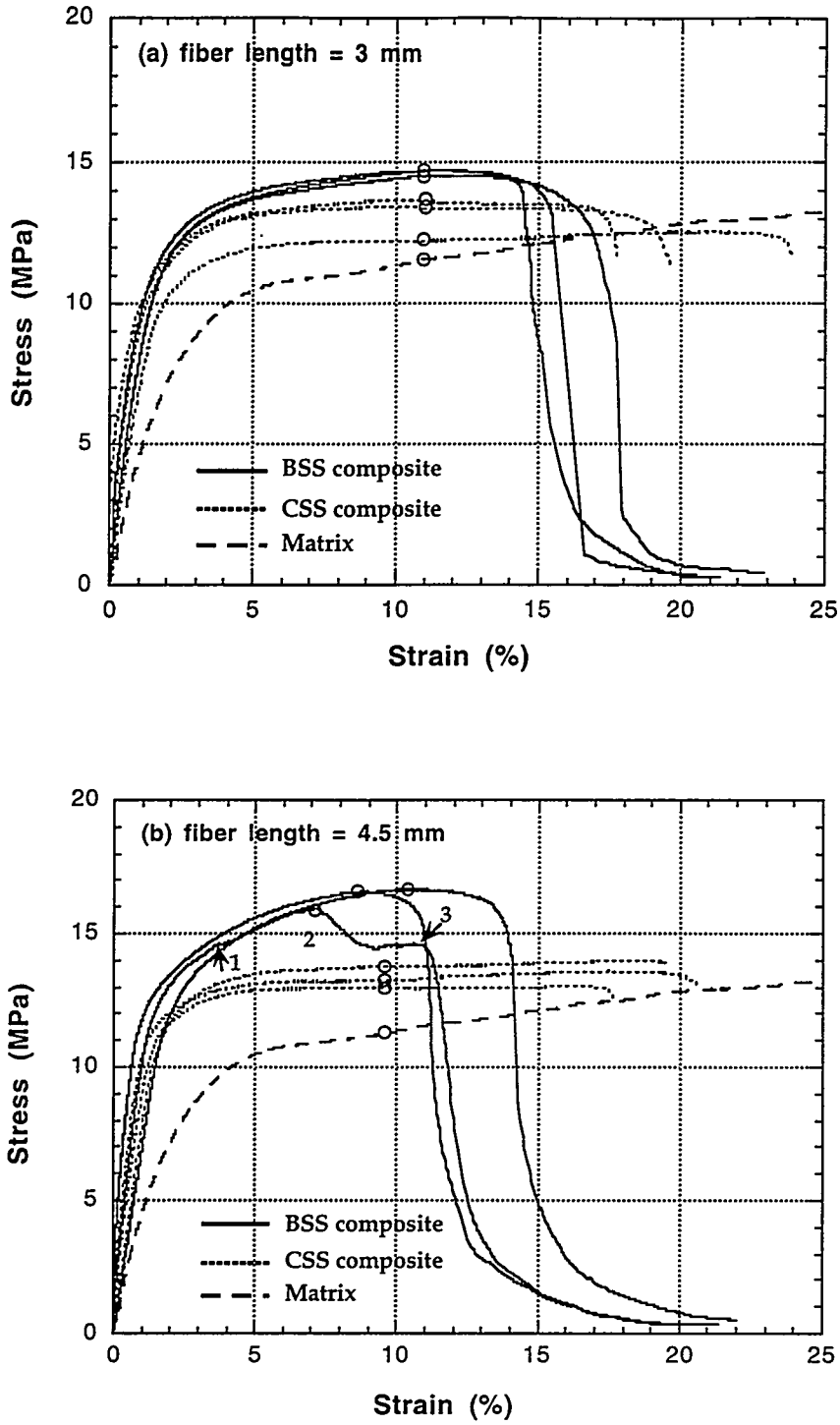

Figure 4: Stress-strain curves of BSS- and CSS-fiber composites and polyester matrix for (a) $\ell = 3$ mm and (b) $\ell = 4.5$ mm.

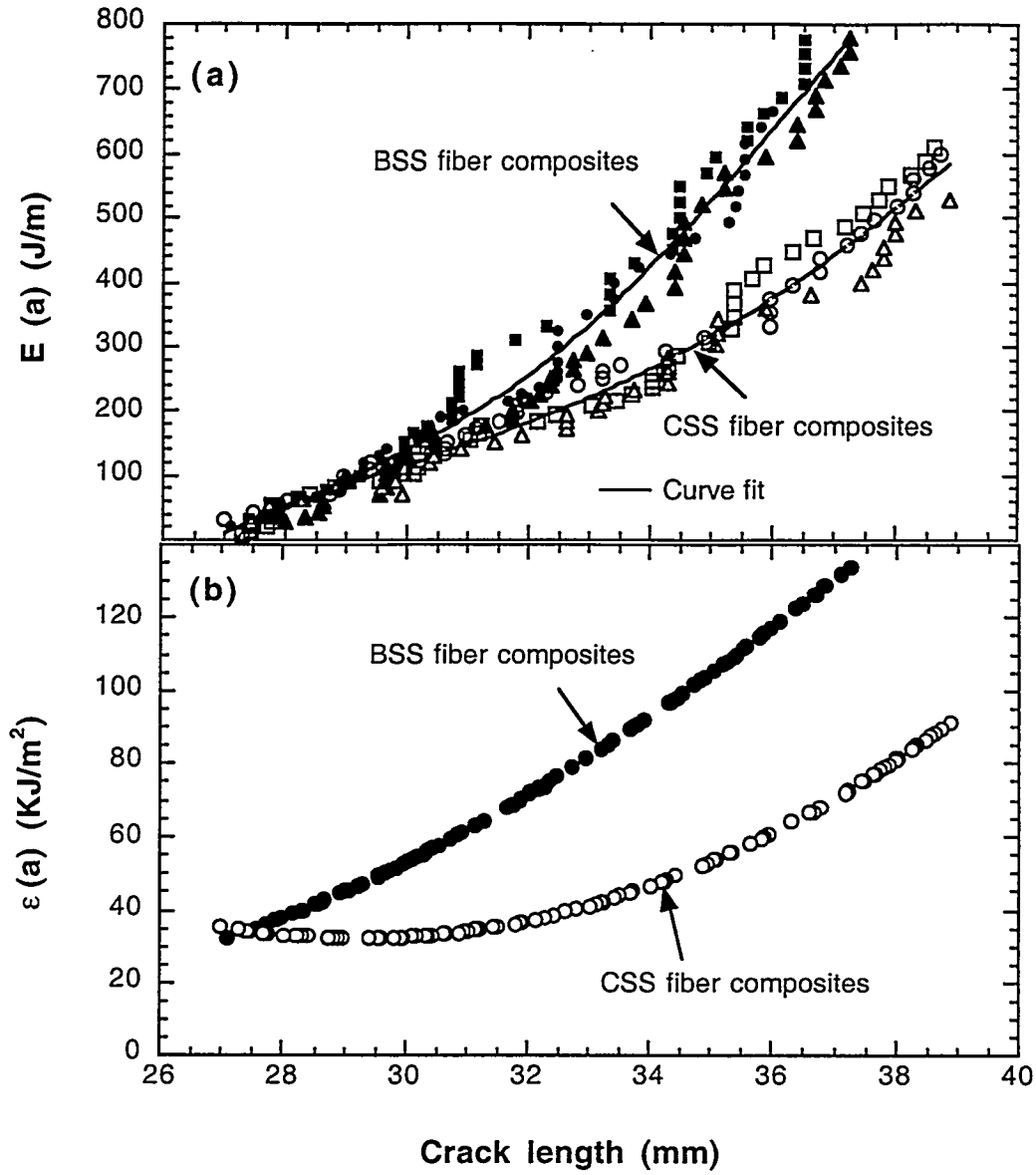

Figure 5: (a) The total normalized energies, E(a) as a function of crack length. The solid and hollow markers represent data points for BSS- and CSS-fiber composites, respectively; (b) the supplied energy for a crack to propagate by a unit length, ε(a), as a function of crack length.

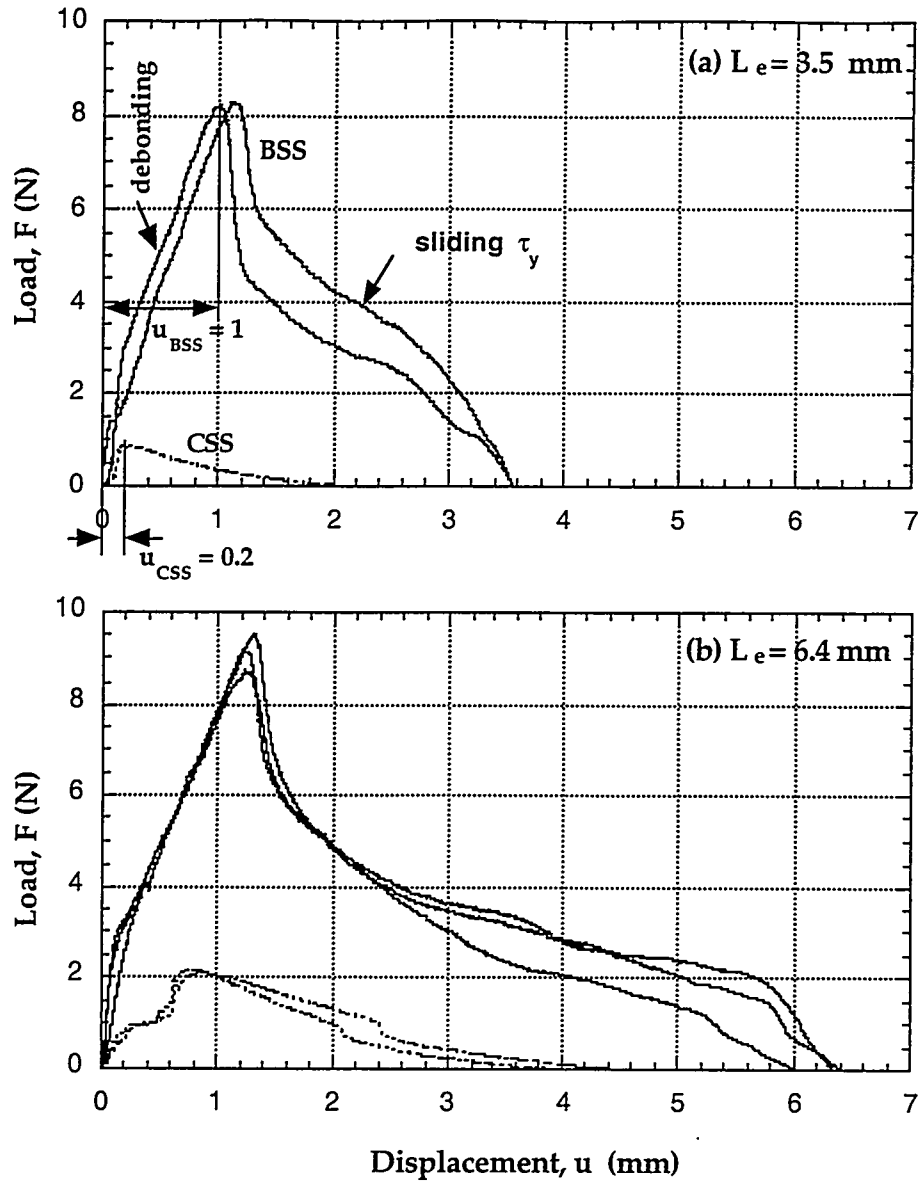

Figure 6: The load-displacement pullout-curves of both BSS and CSS fibers for (a) the embedded length L_e = 3.5 mm and (b) L_e = 6.4 mm.

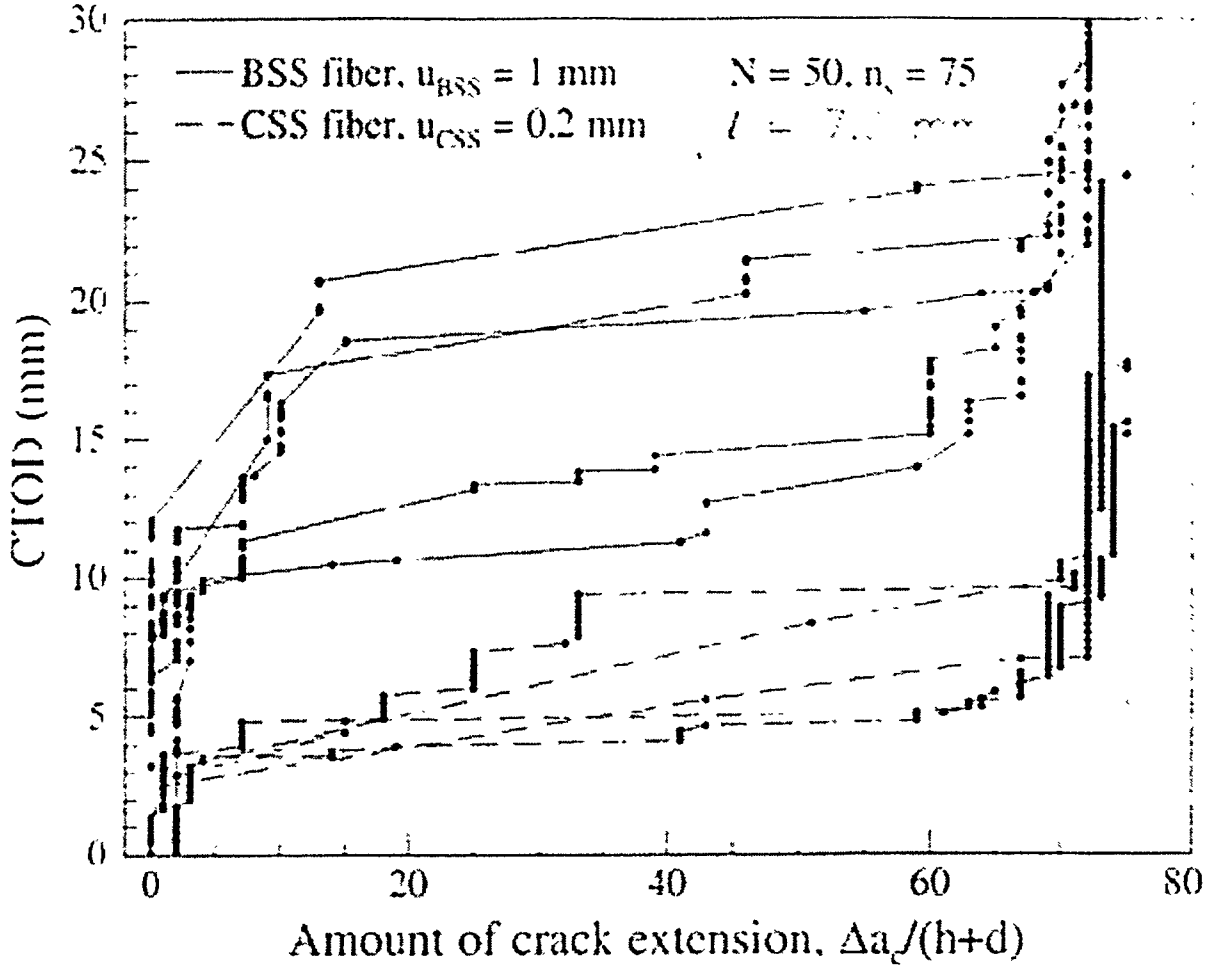

Figure 7: Simulation predictions for the opening displacement (CTOD) at the mouth of the initial notch versus crack extension in five different BSS and CSS-fiber composites with the same short fiber length $\ell = 7.0$ mm.

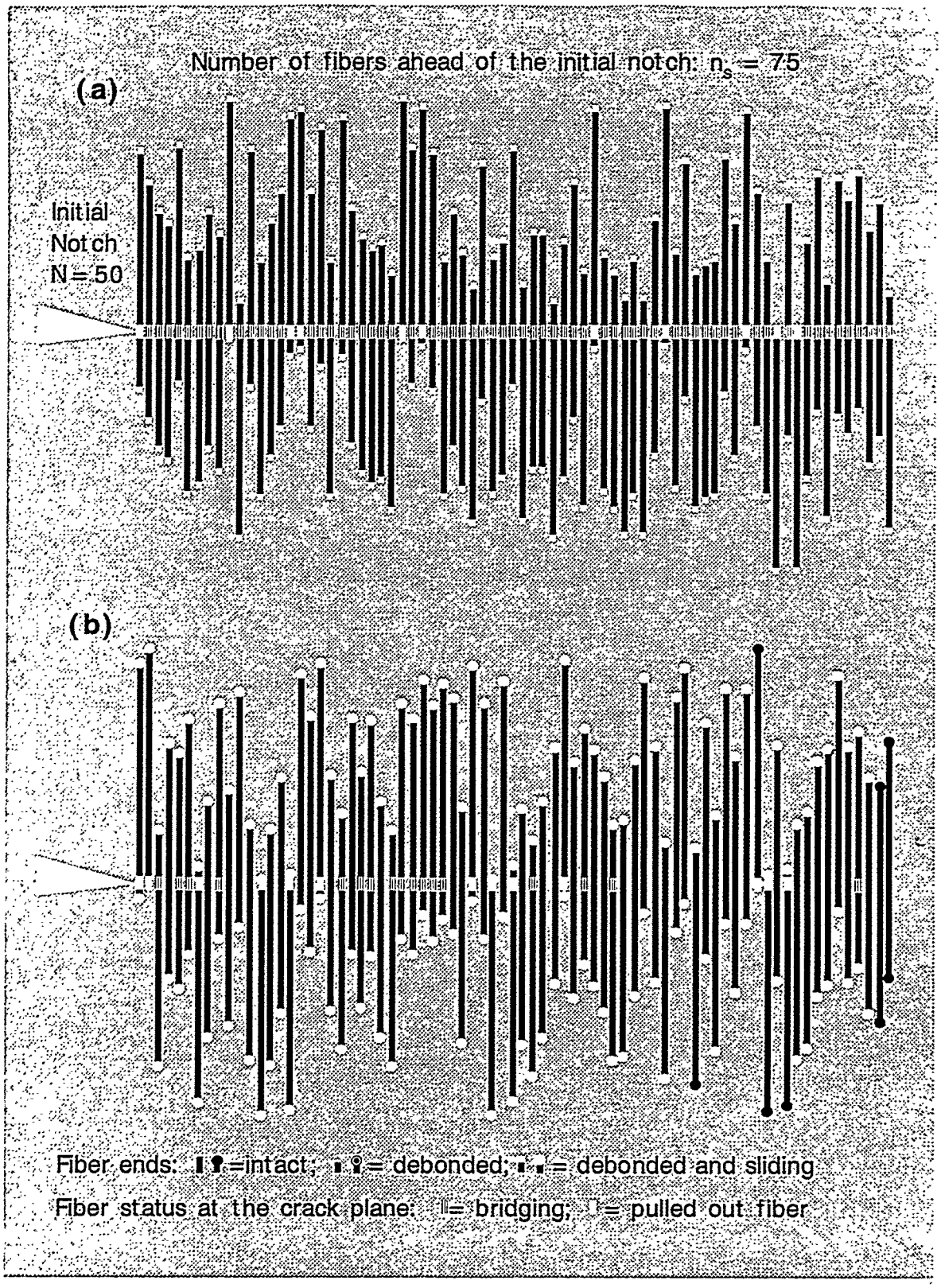

Figure 8: An increment in crack propagation of (a) a CSS fiber composite at normalized applied load = 16.58 and (b) a BSS fiber composite at normalized applied load = 16.91.